Spatio-temporal dynamics of biogeochemical processes and air–sea CO$_2$ fluxes in the Western English Channel based on two years of FerryBox deployment

P. Marrec *, T. Cariou, M. Latimier, E. Macé, P. Morin, M. Vernet, Y. Bozec

CNRS, UMR 7144, Equipe Chimie Marine, Station Biologique de Roscoff, Place Georges Teissier, 29680 Roscoff, France
UPMC Univ. Paris 06, UMR 7144, Adaptation et Diversité en Milieu Marin, Station Biologique de Roscoff, 29680 Roscoff, France

ABSTRACT

From January 2011 to January 2013, a FerryBox system was installed on a Voluntary Observing Ship (VOS), which crossed the Western English Channel (WEC) between Roscoff (France) and Plymouth (UK) up to 3 times a day. The FerryBox continuously measured sea surface temperature (SST), sea surface salinity (SSS), dissolved oxygen (DO), fluorescence and partial pressure of CO$_2$ (from April 2012) along the ferry track. Sensors were calibrated based on 714 bimonthly surface samplings with precisions of 0.016 for SSS, 3.3 μM for DO, 0.40 μg L^{-1} for Chlorophyll-a (Chl-a) (based on fluorescence measurements) and 5.2 μatm for pCO$_2$. Over the 2 years of deployment (900 crossings), we reported 9% of data lost due to technical issues and quality checked data was obtained to allow investigation of the dynamics of biogeochemical processes related to air–sea CO$_2$ fluxes in the WEC. Based on this unprecedented high-frequency dataset, the physical structure of the WEC was assessed using SST anomalies and the presence of a thermal front was observed around the latitude 49.5°N, which divided the WEC in two main provinces: the seasonally stratified northern WEC (nWEC) and the all-year well-mixed southern WEC (sWEC). These hydrographical properties strongly influenced the spatial and inter-annual distributions of phytoplankton blooms, which were mainly limited by nutrients and light availability in the nWEC and the sWEC, respectively. Air–sea CO$_2$ fluxes were also highly related to hydrographical properties of the WEC between late April and early September 2012, with the sWEC a weak source of CO$_2$ to the atmosphere of 0.9 mmol m^{-2} d^{-1}, whereas the nWEC acted as a sink for atmospheric CO$_2$ of 6.9 mmol m^{-2} d^{-1}. The study of short time-scale dynamics of air–sea CO$_2$ fluxes revealed that an intense and short (less than 10 days) summer bloom in the nWEC contributed to 29% of the CO$_2$ sink during the productive period, highlighting the necessity for high frequency observations in coastal ecosystems. During the same period in the sWEC, the tidal cycle was the main driver of air–sea CO$_2$ fluxes with a mean difference in pCO$_2$ values between spring and neap tides of +50 μatm. An extraction of day/night data at 49.90°N showed that the mean day–night differences accounted for 16% of the mean CO$_2$ sink during the 5 months of the study period implying that the diel biological cycle was also significant for air–sea CO$_2$ flux computations. The 2 years of deployment of our FerryBox allowed an excellent survey of the variability of biogeochemical parameters from inter-annual to diurnal time scales and provided new insights into the dynamics of air–sea CO$_2$ fluxes in the contrasted ecosystems of the WEC.

1. Introduction

Traditional surveys of the marine environment using research ships or fixed stations have many limitations in terms of cost and spatio-temporal coverage. Autonomous ocean observing systems mounted on commercial shipping lines, here called FerryBox (www.ferrybox.org), have been developed since the 1990s to overcome these problems. The EU FB5 project "FerryBox" (2002–2005) promoted the development of this tool for operational oceanography and encouraged

European marine institutes to equip Voluntary Observing Ships (VOS) with FerryBox systems. The progress made on FerryBoxes in the last ten years (Hydes et al., 2010; Petersen et al., 2011) proved the efficiency of these cost-effective systems to deliver high frequency physical, chemical and biological data over a wide range of temporal and spatial scales. The installation of a FerryBox on VOS provides the assurance of a continuous energy supply and sheltered conditions inside the ship with easy maintenance during frequent and regular harbour stops. Moreover, the automated cleaning cycles operated by these systems prevent biofouling. The most regular VOS lines are located in marginal seas, which allow monitoring on the same track with frequent time steps in order to follow the variability of the marine environment over short time scales.

* Corresponding author at: CNRS, UMR 7144, Equipe Chimie Marine, Station Biologique de Roscoff, Place Georges Teissier, 29680 Roscoff, France.
E-mail address: pmarrec@sb-roscoff.fr (P. Marrec).

Continental shelf ecosystems are highly dynamic regarding physical, chemical and biological parameters and play a significant role in biogeochemical cycles (Walsh, 1991) despite their relatively moderate size compared to the global oceans (7%). In the context of climate change, with increasing water temperature and rising CO_2 levels in the atmosphere and oceans (IPCC, 2007), long-term high-frequency monitoring of marine ecosystem dynamics is essential, particularly in coastal ecosystems (Goberville et al., 2010). The use of VOS equipped with a FerryBox system with sensors for measurement of partial pressure of CO_2 (pCO_2) is highly recommended to better understand present day carbon cycle dynamics, quantify air–sea CO_2 fluxes and determine future long-term trends in CO_2 in response to climate change forcing (Borges et al., 2010). A limited number of studies have investigated pCO_2 dynamics in coastal ecosystem using VOS automated measurement systems (Omar et al., 2010; Padin et al., 2007; Schneider et al., 2006) and very rarely with high-frequency and long-term pCO_2 and ancillary data records. Access to data on additional physic-chemical and biological parameters such as sea surface temperature (SST), sea surface salinity (SSS), dissolved O_2 (DO), chlorophyll-*a* (Chl-*a*) and nutrient concentrations is essential for studying biogeochemical processes, which control pCO_2 variability at different time scales in coastal ecosystems.

The Western English Channel (WEC) is part of one of the world's largest margins, the North-West European continental shelf. This area is characterized by relatively shallow depths and by intense tidal streams with maximum speeds ranging from 0.5 to 2.0 m s^{-1} (maxima for the entire English Channel (EC)) (Reid et al., 1993). The WEC hosts three different hydrographical structures: all year well-mixed, seasonally stratified and thermal front structures. Such water column characteristics are also observed in adjacent seas of the North-West European continental shelf, i.e. in the Irish Sea and in the North Sea (Hill et al., 2008). Along the French coast (southern WEC (sWEC)), where the tidal currents are the strongest, the water column remains vertically mixed (Wafar et al., 1983), whereas near the English coast (northern WEC (nWEC)), where tidal streams are less intense, seasonal stratification occurs (Smyth et al., 2010). Between these two distinct structures, a frontal zone oscillates, separating well-mixed and stratified waters (Pingree and Griffiths, 1978). In this complex hydrographical context, high-frequency measurements could precisely locate this thermal front and accurately identify the real extent of each hydrographical province. Moreover, previous studies have shown an important spatial and temporal variability of the CO_2 system in the area (Borges and Frankignoulle, 2003; Dumousseaud et al., 2010; Kitidis et al., 2012; Padin et al., 2007). However, these studies were either based on monthly/seasonal measurements on longitudinal transects, or on a fixed station approach (Kitidis et al., 2012), that did not cover both of the hydrographical structures of the WEC.

In the present study, as part of the European cross-border INTERREG IV project MARINEXUS (Our shared seas: Mechanisms of ecosystem change in the Western Channel), we exploited a VOS route between the French and English coasts (Fig. 1) from January 2011 to January 2013, which crosses the different hydrographical structures of the WEC described above. Our FerryBox measurements provided a comprehensive new dataset of SST, SSS, DO, Chl-*a* and pCO_2 in the WEC. In this paper, we first discuss the reliability of the FerryBox data over the two years of deployment. We then describe the physical structure of the WEC based on high-frequency spatio-temporal SST and SSS distributions and assess the environmental conditions driving the dynamics of inter-annual phytoplankton blooms in the different provinces of the WEC. Finally, we present the first high-frequency pCO_2 data acquired across the WEC and discuss the processes driving air–sea CO_2 fluxes from late April 2012 to January 2013 at seasonal to diurnal time scales.
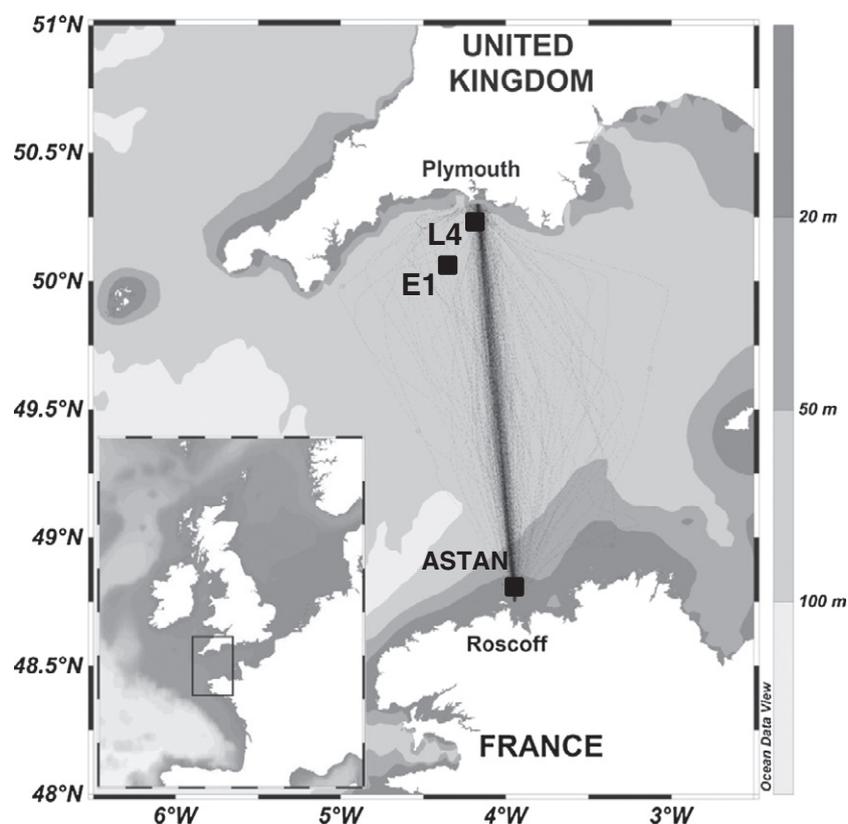
Fig. 1. Map and bathymetry of the study area with the tracks of all crossings made in 2012 (2013 are not shown for the clarity of the figure) between Roscoff (France) and Plymouth (UK). The locations of fixed stations E1 and L4 (Western Channel Observatory), and ASTAN (coastal observatory SOMLIT) are also indicated.

a

b

c

d
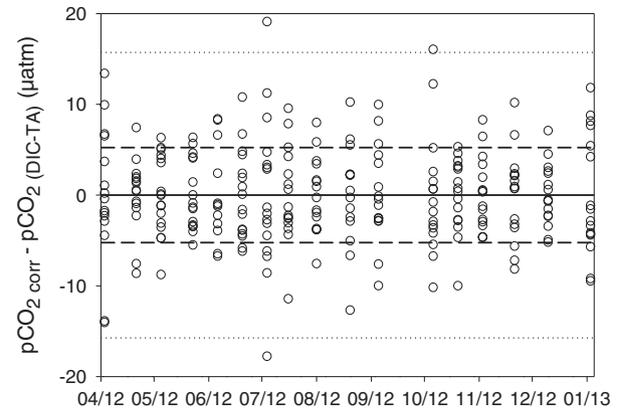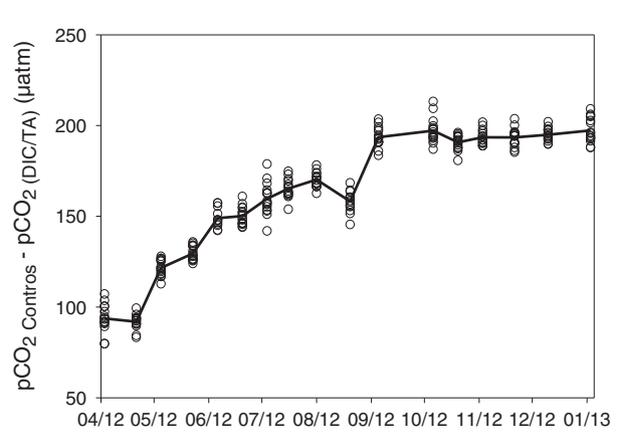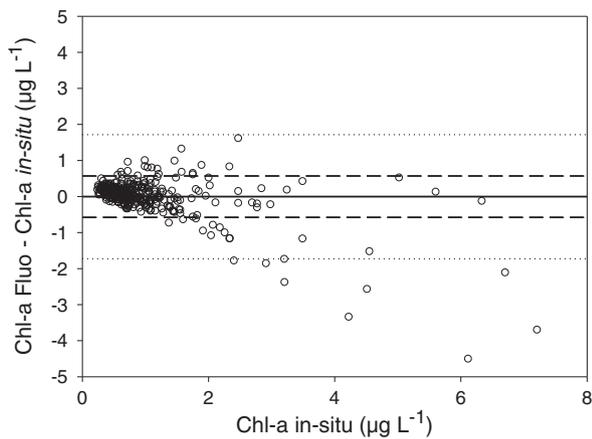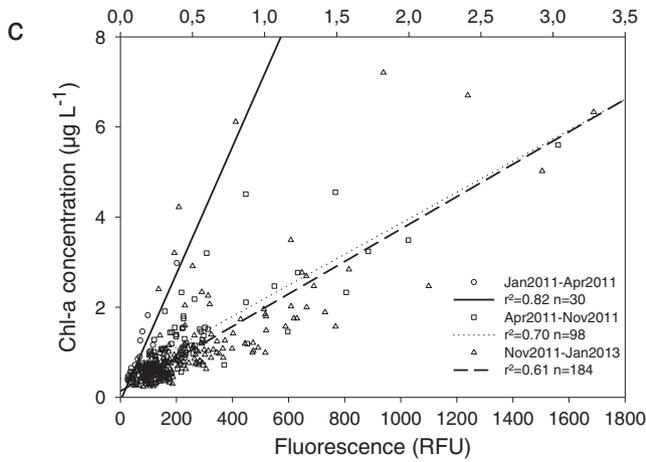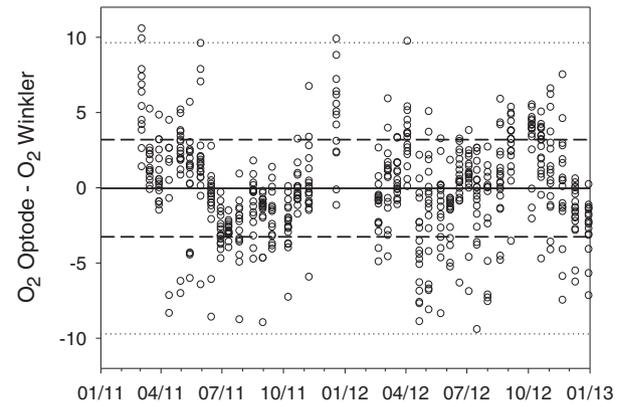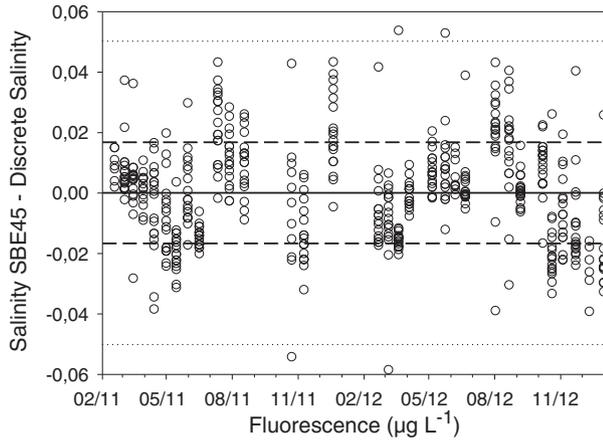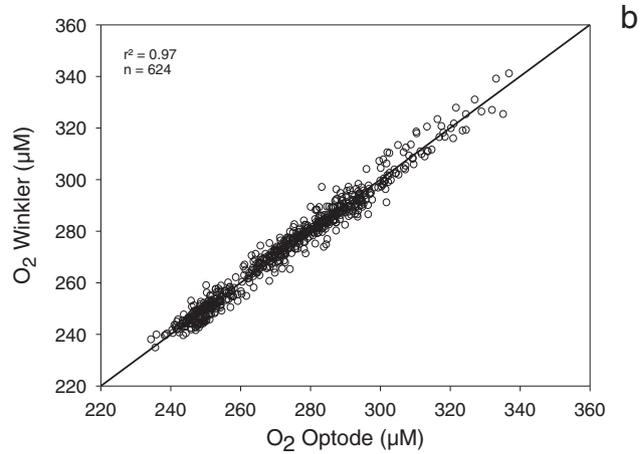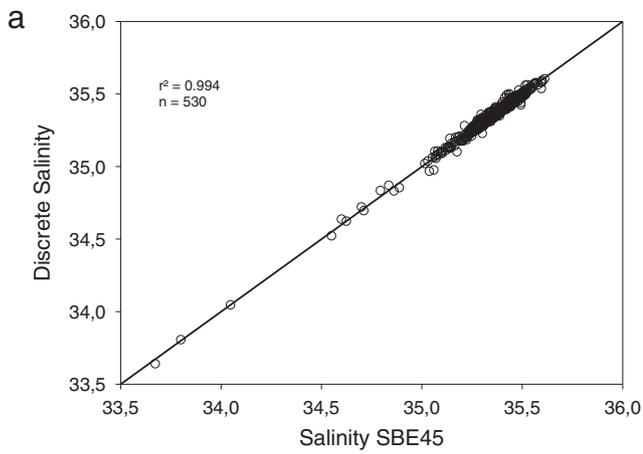
2. Material and methods

2.1. The VOS line and the FerryBox system

In December 2010 we installed a FerryBox system on the Voluntary Observing Ship (VOS) *Armorique* (Brittany Ferries). This vessel crossed the English Channel between Roscoff (France, 48°43′38 N 3°59′03E) and Plymouth (United Kingdom, 50°22′12 N 4°08′31E) (Fig. 1) up to 3 times a day from February to November. The ferry, which does not have a fixed departure/arrival time during the year, crosses the WEC (100 nautical miles) in 6 h during the day and 14 h during the night. A FerryBox is an automated ocean observing system equipped with several sensors. Our FerryBox was built by -4H- JENA and was installed at the engine room level on the *Armorique*. The FerryBox pumped seawater at 4 m depth with a high flow rate to avoid warming of seawater in the water column circuit. The pump was operational only when the ferry was sufficiently far from the harbours to avoid introducing particle-rich waters into the system. The data acquisition of the sensors was performed every minute under a LabView environment and data were automatically sent and stored in our database in Roscoff at the end of each crossing. From January 2011 to January 2013 the ferry performed more than 900 crossings with data acquisition.

A Sea Bird SBE 38 temperature sensor recorded the in-situ seawater temperature with a precision of 0.001 °C and a Sea Bird SBE 45 thermosalinograph recorded the temperature and salinity inside the seawater circuit of the Ferry Box with precisions of 0.002 °C and 0.005, respectively. Dissolved oxygen concentrations were measured using an Aanderaa Optode 3835 and a Turner Designs C3 fluorometer measured chlorophyll-*a* fluorescence. From April 2012 a Contros HydroC/CO_2 FT sensor was used for measurements of the partial pressure of CO_2 (pCO_2) in seawater. This sensor measured the pCO_2 continuously in a headspace behind a membrane equilibrator with a non-dispersive infra-red detector (Fietzek and Körtzinger, 2010). Sensors were calibrated and/or adjusted based on bimonthly discrete measurements made on the ferry (see Section 3.1.).

2.2. Bimonthly discrete sampling

Between January 2011 and January 2013, discrete sampling was performed on 40 return crossings between Roscoff and Plymouth with a total of 714 sampling locations in the WEC. During each cruise, 18 water samples were taken from the FerryBox seawater circuit for the determination of dissolved oxygen (DO), dissolved inorganic carbon (DIC), total alkalinity (TA), nutrients (NO_3^-, NO_2^-, PO_4^{3-} and SiO_4^-), chlorophyll-*a* (Chl-*a*) and salinity. Discrete salinity samples were measured on a portasal salinometer at the SHOM (Service Hydrographique et Oceanographique de la Marine) with a precision of 0.002. DO concentrations were determined within a week of sampling by the Winkler method using a potentiometric end-point determination with an estimated accuracy of 0.5 μmol L^{-1}. The oxygen saturation level (DO%) was then calculated according to Weiss (1970) from the observed DO and the DO at saturation using the in-situ temperature and salinity data. In 2011, DIC and TA were collected in 100 mL and 250 mL borosilicate glass bottles, respectively, poisoned with 100 μL of saturated HgCl$_2$, and analysed within a week of sampling. DIC was determined with an AIRICA system (Marianda Inc.) after acidification of a 2.3 mL aliquot with phosphoric acid, extraction by a carrier gas (N_2) and detection with a LICOR-7000 IR detector. TA was measured with a TA-ALK 2 system (Appolo SciTech.) by the Gran electro-titration method on 25 mL

aliquots. The accuracies of DIC and TA measurements were determined with Certified Reference Materials (CRM) provided by A. G. Dickson, Scripps Institution of Oceanography (Batch 92). CRM standards were measured at the start and at the end of each day of analysis and every 10 samples during the runs. Accuracies of the DIC and TA measurements were 1.5 μmol kg^{-1} and 3 μmol kg^{-1}, respectively, based on bi-annual measurements of different batches. In 2012, because of the large amount of samples collected, we chose to analyse DIC and TA at the national facility for analysis of carbonate system parameters (SNAPO-CO_2, LOCEAN, Paris), which allows simultaneous measurements of DIC/TA by potentiometric titration. DIC and TA were collected in 500 mL borosilicate glass bottles, poisoned with 300 μL of HgCl$_2$, stored at 4 °C and analysed simultaneously by potentiometric titration derived from the method developed by Edmond (1970) using a closed cell. The calculation of equivalence points was done using a non-linear regression (DOE, 1994). These simultaneous DIC and TA analyse were performed at the SNAPO-CO_2 with an accuracy of ±2 μmol kg^{-1} for DIC and TA. Inter-calibration between the two DIC methods and two TA methods confirmed the accuracies of TA and DIC of ±2 μmol kg^{-1} and ±3 μmol kg^{-1}, respectively. To determine chlorophyll-*a* concentrations (Chl-*a*), 0.5 L of seawater were filtered through glass-fibre filters (Whatman GF/F) and immediately frozen. Samples were extracted in 5 mL of acetone. Correction for phaeopigments was carried out using the acidification method with an HCl solution, after primary fluorescence measurements using a fluorometer (Turner Designs model 10 AU digital fluorometer) to calculate Chl-*a* concentrations according to EPA (1997). The estimated accuracy was 0.05 μg L^{-1}. Nutrient concentrations (NO_3^-, NO_2^-, PO_4^{3-} and SiO_4^-) were determined using an AA3 auto-analyser (AXFLOW) following the method of Aminot and Kérouel (2007) with accuracies of 0.02 μg L^{-1}, 1 ng L^{-1}, 1 ng L^{-1} and 0.01 μg L^{-1} for NO_3^-, NO_2^-, PO_4^{3-} and SiO_4^-, respectively.

2.3. CO_2 system and air–sea CO_2 fluxes calculation

Seawater pCO_2 values were calculated from TA, DIC, temperature, salinity and nutrient concentrations with the CO2SYS programme (Pierrot et al., 2006) using the equilibrium constants of CO_2 proposed by Mehrbach et al. (1973), refitted by Dickson and Millero (1987) on the seawater pH scale, as recommended by Dickson et al. (2007). The computed values of pCO_2 from DIC and TA have an uncertainty of ±5.8 μatm (Zeebe and Wolf-Gladrow, 2001), which does not include uncertainties in the dissociation constants and ignores the contribution of organic compounds to alkalinity (Koeve and Oschlies, 2012, Hoppe et al., 2012). The WEC waters are open continental shelf waters, which are weakly influenced by estuarine plumes. Organic matter levels are thus low, except in the vicinity of Plymouth. Organic compounds therefore do not significantly influence alkalinity in most of the WEC. The calculated pCO_2 values allowed us to adjust the Contros HydroC/CO_2 FT data (see Section 3.1.). Atmospheric pCO_2 ($pCO_{2\ air}$) was calculated from the CO_2 molar fraction (xCO_2) at the Mace Head site (53°33′N 9°00′W, southern Ireland) of the RAMCES network (Observatory Network for Greenhouse gases) and from the water vapour pressure (pH_2O) using the Weiss and Price (1980) equation. Atmospheric pressure (Patm) in the middle of the WEC (49°50′N, 4°00′W) was obtained from the NCEP/NCAR re-analysis project (Kalnay et al., 1996).

The fluxes of CO_2 across the air–sea interface (F) were computed from the pCO_2 air–sea gradient ($\Delta pCO_2 = pCO_{2water} - pCO_{2air}$, μatm) according to:

$$F = k * \alpha * \Delta pCO_2 \tag{1}$$

Fig. 2. Adjustment of high frequency data of (a) SSS, (b) DO, (c) Chl-*a* and (d) pCO_2 based on bimonthly discrete measurements. For SSS and DO, top plots show the discrete measurements versus corrected sensor values. For Chl-*a*, the top plot shows the discrete measurements versus fluorescence in relative fluorescence units (RFU) and, during the third deployment, versus fluorescence data converted into Chl-*a* concentration by the C3 software. For pCO_2, top plot shows the differences between pCO_2 data from the HydroC/CO_2 FT sensor before correction and pCO_2 calculated from DIC/TA discrete measurements (μatm) during the deployment of the sensor. Bottom plots show differences between sensor values and discrete measurements over time. Dashed lines represent standard deviation of the differences between sensor values and discrete measurements whereas dotted lines represent three times the standard deviation.
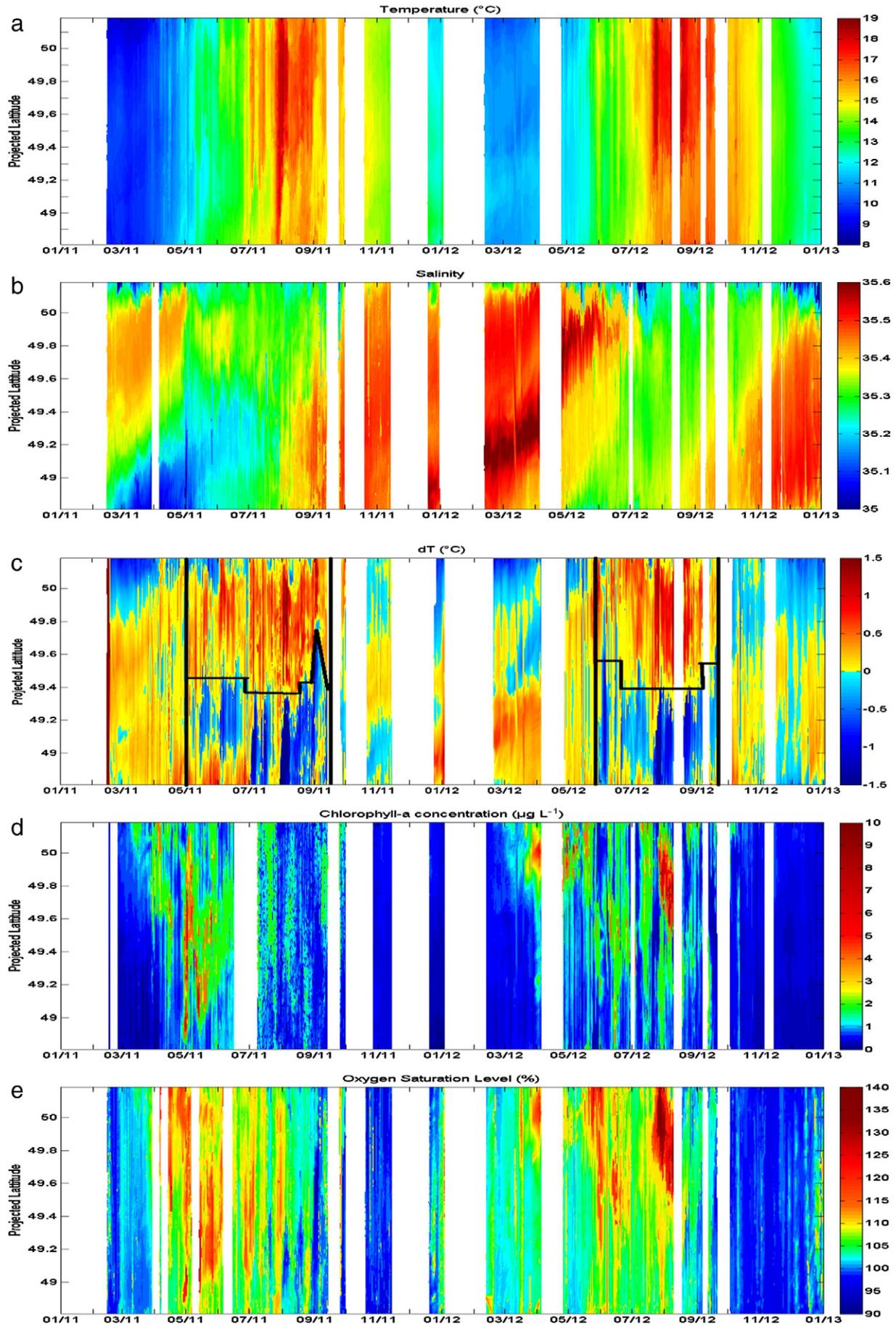
where k is the gas transfer velocity (m s^{-1}) and α is the solubility coefficient of CO_2 (mol atm^{-1} m^{-3}) calculated after Weiss (1970). The exchange coefficient k was computed as a function of wind speed with the algorithm given by Nightingale et al. (2000) established in the Southern Bight of the North Sea (SBNS):

$$k = \left(0.222 * u_{10}^2 + 0.333 * u_{10}\right) * (Sc/660)^{-0.5}$$

where u_{10} is the wind speed data at 10 m height (m s^{-1}) and Sc the Schmidt number at in-situ SST. The SBNS and the WEC present similar environmental characteristics: these two shallow continental shelves are both close to land with high tidal currents controlling the physical structure of the water column. Wind speeds along the ferry track were extracted from daily wind speed data corrected at 10 m height from the NCEP/NCAR re-analysis project provided by the NOAA-ESRL Physical Sciences Division, (Boulder, CO, USA, http://wwww.esrl.noaa.gov/psd/).

3. Results and discussion

3.1. Reliability of the FerryBox system

From January 2011 to January 2013, the correlation between 530 discrete SSS samples and sensor data was very robust (Fig. 2a). Two SBE45 sensors calibrated using the SHOM (Service Hydrographique et Océanographique de la Marine) calibration facility were rotated in order to prevent sensor drift during the two-year deployment. During the deployment of the second SBE45 sensor from April 2011 to January 2013, we observed a temporal drift (-0.00013 PSU day^{-1}, n = 472, $r^2 = 0.78$) and corrected the raw data. With regular maintenance and calibration by discrete measurements, high precision (0.016) and long-term stability in SSS measurements was attained on our FerryBox (Fig. 2a).

Over the two-year sampling period, two Optodes were used. We applied salinity and temperature corrections to the raw Optode data using the Aanderaa correction methods. Fig. 2b shows the correlation between sensor data corrected to in-situ SST and SSS and from inherent sensor offsets during each deployment, versus the discrete measurements (n = 653, $r^2 = 0.97$, Fig. 2b). We obtained a precision of 3.3 μM based on the standard deviation of residuals of similar range as reported by Hydes et al. (2009) also on a FerryBox system (3 to 5 μM), this being lower than the accuracy stated by the manufacturer (8 μM or 5%). We observed abnormally high positive residual differences during two crossings (February 2011 and December 2011) (Fig. 2b). During these crossings the sea was particularly rough and many bubbles were observed inside the seawater circuit, which might be due to our water inlet being too shallow for very rough seas. During several crossings, we observed a few highly negative residuals. There was no clear explanation for these values, which might be related to sampling operations or quality of the Winkler reagents during given transects. Our results indicate that Aanderaa Optodes are suitable sensors for long-term deployment on a FerryBox when the Optode sensor is regularly rotated to avoid major sensor drift.

Fig. 2c shows the correlation between sensor data and discrete Chl-*a* measurements for the three deployments of C3 instruments. Two C3 sensors were used from January 2011 to January 2013 with two rotations during this period. During the two first deployments we recorded fluorescence in relative fluorescence units (RFU) and during the third deployment fluorescence data were converted into Chl-*a* concentration by the C3 software. The most significant correlation between FerryBox data and discrete measurements was observed from January 2011 to April 2011, with an r^2 of 0.82 from 30 measurements. Between April 2011 and November 2011 and between November 2011 and January 2013 correlations were weaker, but still significant with an r^2 of 0.70 and 0.61, respectively. The use of fluorescence data converted into Chl-*a* concentration was based on laboratory calibration of the C3 sensor using a phytoplankton culture. This single specy calibration is probably not representative of the phytoplankton diversity of the natural system, potentially inducing errors in the estimated Chl-*a*. After correction of raw fluorescence data (in RFU and in μg L^{-1}) by the respective linear regression coefficients, we plotted the differences of corrected estimates of Chl-*a* and Chl-*a* concentrations measured in the laboratory versus the Chl-*a* laboratory measurements (Fig. 2c). Between 0 and 3 μg L^{-1}, the Chl-*a* difference is homogeneously distributed around 0 with a standard deviation of 0.36 μg L^{-1}. Beyond 3 μg L^{-1} important deviations from 0 were observed. The potential sources of error might be due to the different phytoplankton species composition in WEC surface water in different seasons (Guilloux et al., 2013; Southward et al., 2005) and/or the effect of fluorescence quenching (Xing et al., 2012) since most of the crossings were performed during daytime. Despite the high standard deviation, high-frequency fluorescence data do permit the use of Chl-*a* variations as an indicator of the presence of phytoplankton in surface waters of the WEC.

The HydroC/CO_2 FT pCO$_2$ sensor was installed on the FerryBox in April 2012. We applied the algorithm of Takahashi et al. (1993) to the sensor data to correct for the warming of seawater inside the seawater circuit using the differences between in-situ and seawater-circuit temperature. Between April 2012 and January 2013, we analysed 264 DIC and TA samples to calculate pCO$_2$ values. The difference between sensor pCO$_2$ data and discrete measurements of pCO$_2$ through time allowed us to estimate the drift of the sensor (Fig. 2d). This drift was not always linear; we corrected the high-frequency data using step-by-step interpolations between each crossing from the bimonthly offsets observed. Regular zeroing can also be performed to follow any potential drift of the instrument with time, but software issues during our deployment prevented access to this procedure. The origin of the high offset (90 μatm) observed at the beginning of the deployment is not well defined. One month before the deployment, immediately after the manufacturer calibrated the HydroC/CO_2 FT, we tested this sensor in the laboratory against a classical equilibration system with IR detection (LICOR 7000) (Bozec et al., 2012). These tests did not show any significant offset between the two types of measurements. The HydroC/CO_2 FT was then stored for one month prior to its installation on the FerryBox. The one-month storage period and new environmental conditions might explain the high offset observed at the beginning of the deployment (Fig. 2d). The pCO$_2$ values during the deployment ranged between 160 μatm and 460 μatm. The difference between corrected sensor data and discrete measurements through time (Fig. 2d) had a standard deviation of 5.2 μatm which was better than the level of deviation announced by the manufacturer, which is ±1% of upper range value (200 to 1000 μatm, thus 10 μatm). To the best of our knowledge this was the first time that the Contros HydroC/CO_2 FT sensor has been deployed on a FerryBox system and it was a relatively long deployment compared to other studies using this sensor (Fiedler et al., 2013; Saderne et al., 2013). This sensor proved to have sufficient reliability to study pCO$_2$ variability in dynamic coastal ecosystems, which exhibit a wide range of pCO$_2$ values (150–500 μatm). However the precision obtained with this sensor was low compared to state-of-the-art pCO$_2$ analyzers. The maintenance and calibration of the Contros HydroC/CO_2 FT sensors are relatively simple and low cost, and we believe the data quality obtained with this sensor will be improved by setting up routine

Fig. 3. Surface distributions of (a) SST (°C), (b) SSS, (c) SST anomaly (°C), (d) Chl-*a* (μg L^{-1}) and (e) DO% in the WEC between Roscoff and Plymouth for the years 2011 and 2012. On Fig. 3c, the horizontal black lines represent an estimate of the location of the thermal front; the vertical black lines approximately delimit the period when stratification occurred in the northern WEC.

zeroing values with the manufacturer to more accurately estimate the drift of the sensor.

Automated ocean observing systems such as the FerryBox are subject to technical issues inherent to high-technology equipment deployed in challenging environments over long periods. During the two years of deployment, we limited the data loss due to technical issues to 9%. The proximity of the ferry terminal to our laboratory and the high frequency of crossings facilitated rapid intervention on technical issues and were major benefits to avoid extended periods of instrument downtime. We thus obtained a very comprehensive dataset, with sufficient precision to allow assessment of the dynamics of biogeochemical processes and air–sea CO_2 fluxes in the WEC.

3.2. Observation of the physical structure of the WEC

Previous studies (e.g. Pingree and Griffiths, 1978) have shown that the WEC is characterized by the presence of a thermal front from late spring to early fall, which periodically separates the two main provinces, the northern WEC (nWEC) and the southern WEC (sWEC). Measurements undertaken by coastal observatories on either side of the WEC (Fig. 1) have been used to describe the physical structure of the water column at fixed stations representative of each province. Station E1 (50.03°N 4.37°W; depth 75 m; Western Channel Observatory) is representative of seasonally stratified open shelf seas of the nWEC (Smyth et al., 2010). The Astan station (48°46′40 N 3°56′15 W; depth 60 m; Roscoff Coastal Observatory (SOMLIT)) is representative of an all-year well-mixed water column system of the sWEC as described by Wafar et al. (1983).

Fig. 3a shows SST distribution in the WEC from high-frequency FerryBox measurements from the 14th of February 2011 to the 31st of December 2012. SST followed classical dynamics with warmer surface waters from spring to summer and cooling from autumn to winter. The coolest SST was recorded in February 2011 (8.2 °C) close to the English coast and the warmest SST was recorded in late July 2011 (19.4 °C). In both years the coolest STTs were observed in the nWEC close to the English coast and the warmest SSTs in the nWEC stratified waters. Winter and early spring 2011 were colder than in 2012. The mean annual temperature amplitudes were approximately 10 °C.

Fig. 3c shows SST anomalies (dT) obtained from the difference between SST and mean SST from running averages performed on 500 consecutive SST measurement steps (a crossing corresponded to approximately 300–400 min or steps). dT allowed us to distinguish the two main hydrographical provinces in the WEC. For each SST step a mean SST was calculated from the 500 next SST records. The mean SST was thus always different but represented the mean SST of each transect. From mid-spring to early autumn, negative dT values were related to the coolest waters of the well-mixed sWEC and positive dT values were related to the seasonally stratified nWEC waters. FerryBox high-frequency measurements clearly reveal the presence and the oscillations of a thermal front separating the two provinces. The mean position of the thermal front (horizontal black line on Fig. 3c) was located between 49.4°N and 49.6°N. The highest positive and negative dT values were observed during summer when the differences in SST between nWEC and sWEC were the most marked. In 2011, differentiation between the two provinces was first observed in early May and one month later in 2012. Fig. 3a shows that warming of surface waters started earlier in 2011 than in 2012 and this explains the one-month delay in 2012 in the separation of the WEC to northern and southern provinces. The end of separation between the two provinces occurred in mid-September for both years. In the following sections, all references to nWEC and sWEC will be based on the SST anomaly distinguished on Fig. 3c.

In addition to SST distribution across the WEC, high-frequency SSS measurements provided details on the physical structure of the WEC. Fig. 3b shows the distribution of SSS across the WEC over the years 2011 and 2012. Maximum SSS values (>35.50) were recorded from

autumn 2011 to spring 2012 in the entire WEC except near the English coast. During almost all the year low salinities (<35.3) were observed near the coast at a latitude north of 50°N due to freshwater inputs from the Plymouth rivers. In July 2012, freshwater inputs from these rivers decreased SSS even further south of 49.9°N. In the southern part of the WEC, from February to June 2011, low salinity (<35.30) surface waters were also observed and salinity dropped below 35.10 (Fig. 3b). According to Kelly-Gerreyn et al. (2006), low saline waters from the Loire plume can reach the southern part of the WEC and these coastal waters are also influenced by freshwater discharges from Britanny rivers. In 2012, such low saline surface waters were not recorded, but some minor freshwater inputs lowered SSS off the French coast during spring. Negative dT anomalies were recorded up to 50°N and were related to these freshwater inputs (Fig. 3c), which have lower SST than seasonally stratified open shelf waters of the nWEC. Therefore, from SSS observations, a third zone could be distinguished along the English coast in addition to the two mentioned above.

3.3. Inter-annual dynamics of phytoplankton blooms

DO%, which can be used as an indicator of biological processes, and Chl-a distribution patterns showed clear similarities during 2011 and 2012 in the WEC (Fig. 3d and e). During winter, Chl-a concentrations were lower than 0.5 μg L^{-1} and DO% values were close to equilibrium (100%). During both years, the productive period, marked by Chl-a increase, started more than one month earlier in the nWEC than in the sWEC and DO% oversaturations followed these Chl-a increases. This delay was mainly due to the fact that in the nWEC the tidal streams were lower than in the south (Pingree and Griffiths, 1978) and the stratification of the water column occurred when surface seawater heated up, as seen above, with the installation of the thermal front (Fig. 3c). These two factors allowed phytoplankton to benefit from better light conditions in the nWEC than in the sWEC with the installation of a euphotic zone. Surface waters of the WEC remained oversaturated in DO compared to the atmospheric equilibrium for the duration of the productive period. After the productive period, the remineralization phase started as seen from DO% undersaturation, high NO_2^- concentrations and low Chl-a values (Figs. 3e, 4d and 3d). In 2011 and 2012, dominant heterotrophic processes were first observed in the sWEC and more than one month later in the nWEC. The remineralization processes, occurring mainly in deeper waters and at the sediment interface, affected the entire water column in the sWEC. In the nWEC, these processes took place under the mixed layer depth and only affected the surface waters after the breakdown of the thermocline. This might explain why dominant heterotrophy was observed first in the sWEC. From the distribution of DO% and Chl-a in these two contrasted provinces (Fig. 3c) it clearly appeared that hydrographical properties of the water column strongly influenced the seasonal phytoplankton bloom distributions and production/remineralization processes.

The two years of FerryBox records allowed us to observe important inter-annual variations and significant differences between the seasonally stratified nWEC and the all-year well-mixed sWEC.

The most significant inter-annual variation was observed in the sWEC. In 2011 an important spring bloom occurred from May to June (Fig. 3d and e), whereas in 2012 no such intense phytoplankton bloom was observed at this time. Fig. 4 shows that in 2011 the winter pool of nutrients decreased abruptly once the bloom started with significant consumption of SiO_4^- in May and total NO_3^- depletion in July. In 2012 the decrease was less important: NO_3^- was not totally depleted during the summer period and SiO_4^- did not significantly decrease. In 2012, nutrient availability was not the limiting factor for phytoplankton blooms and phytoplankton blooms did not deplete nutrient concentrations like in 2011. As reported by previous studies, the main factor controlling the phytoplankton production in the well-mixed waters of the WEC is the light availability (Boalch et al., 1978; L'Helguen et al., 1996; Wafar et al., 1983). During our study period, we observed variable
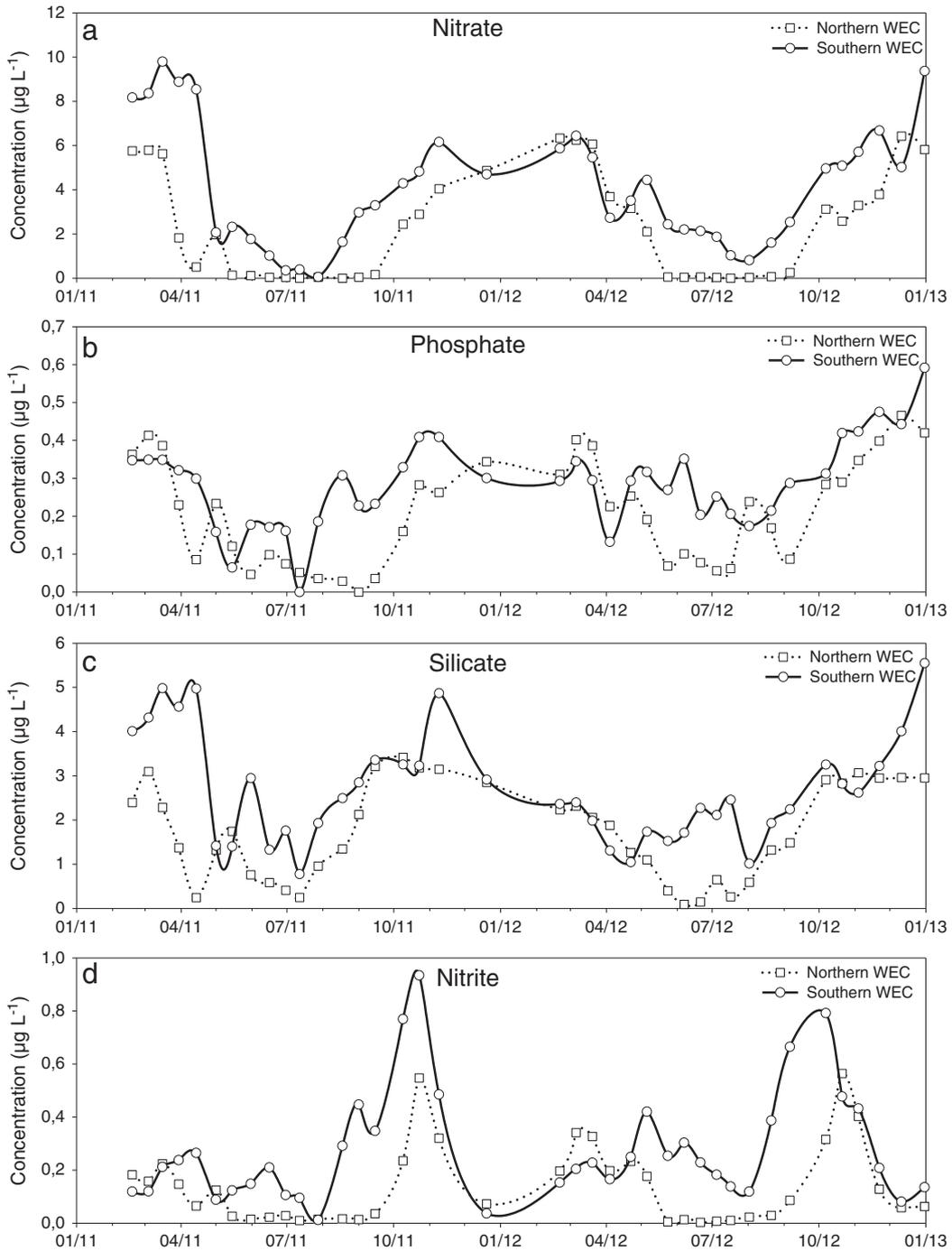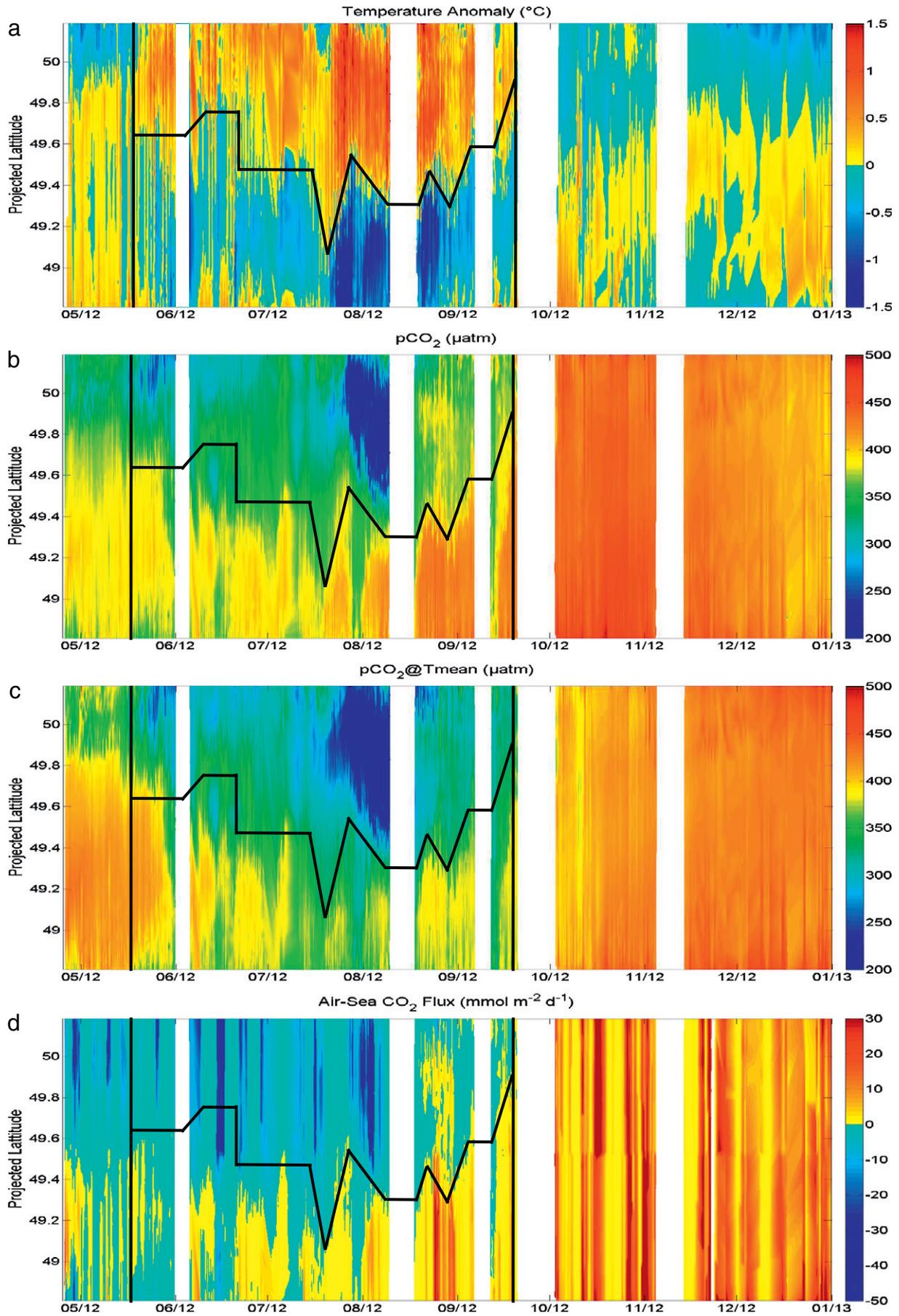
Fig. 4. NO_3^- (a), PO_4^{3-} (b), SiO_4^- (c) and NO_2^- (d) concentrations ($\mu g\ L^{-1}$) in 2011 and 2012 at 48.9°N (representative of the southern WEC, black line, empty circles) and at 49.9°N (representative of the northern WEC, dashed lines, empty squares) from bimonthly discrete measurements.

meteorological conditions throughout the years. These variable meteorological conditions controlled directly the light availability, which was likely the main factor responsible for the strong inter-annual variability of phytoplankton blooms in the sWEC.

In the nWEC, inter-annual variations were also observed, especially in the intensity and chronology of blooms. From April to June 2011, a succession of blooms occurred and DO% remained strongly oversaturated (>110%) even when surface Chl-*a* concentrations were low. Following the first spring phytoplankton blooms, surface NO_3^- was totally depleted until the end of the productive period (Fig. 4a). The second spring phytoplankton bloom in 2011 might be linked to a freshwater input (Fig. 3b), which brought nutrients in early May (Fig. 4) when they were almost

depleted. DO% remained relatively high even when surface Chl-*a* concentrations were low during the productive period. These observations suggest the presence of a sub-surface phytoplankton bloom above the thermocline after nutrient depletion in the surface layer, as reported previously by Southward et al. (2005) and by Smyth et al. (2010). After the spring blooms, we observed extremely low NO_3^- and SiO_4^- concentrations in the surface waters. However, as observed by Smyth et al. (2010), these nutrients might still be available at the thermocline and allow sub-surface phytoplankton blooms at the interface between deep and surface waters. This might explain the relatively high DO% observed even when surface Chl-*a* concentrations were low. Moreover Chl-*a* values are representative of phytoplankton stocks but not always of

a — Temperature Anomaly (°C)

b — pCO$_2$ (µatm)

c — pCO$_2$@Tmean (µatm)

d — Air-Sea CO$_2$ Flux (mmol m^{-2} d^{-1})

their biological activity, which can be indicated by DO%. In 2012, the early spring bloom was more intense than in 2011 (Fig. 3d), but less extended in time and space over the following weeks. After the initial 2012 spring bloom, NO_3^- and SiO_4^- were also totally depleted and PO_4^{3-} decreased significantly (Fig. 4). However, from the end of July to mid-August 2012 a third massive phytoplankton bloom (Chl-a >10 µg L^{-1}) was recorded, followed by the highest DO% (>135%) values observed. During this period, NO_3^- was totally depleted but we observed an increase in PO_4^{3-} (Fig. 4a and b). Fig. 3b clearly shows freshwater inputs from the English coast in July 2012, which might have provided an input of nutrients to the nutrient-depleted nWEC surface waters. In the nWEC, the main limiting factor for phytoplankton growth was nutrient availability. The lower tidal streams compare to the sWEC and the stratification of the water column allowed phytoplankton to benefit from better light availability in contrast to the all-year well-mixed sWEC. The short time-scale dynamics of these blooms and their impact on air–sea CO_2 fluxes are discussed in Section 3.4.

3.4. Short time-scale dynamics of pCO₂ and air–sea CO₂ fluxes

Fig. 5 shows the spatio-temporal distribution of the SST anomaly (Section 3.2.), of partial pressure of CO_2 (pCO₂, in µatm), of pCO₂ normalized to the mean temperature of 13 °C (pCO₂@Tmean) according to Takahashi et al. (1993) and of air–sea CO_2 fluxes (in mmol m^{-2} d^{-1}) in the WEC between the end of April 2012 and January 2013. The pCO₂ values were adjusted from bimonthly discrete measurements (see Section 3.1.). During the first half of the sample period, the contrast between the seasonally stratified nWEC and the all-year well-mixed sWEC was clear.

In the nWEC, from April to September 2012, surface seawater was strongly undersaturated in CO_2 compared to the atmospheric equilibrium and during this period the nWEC acted as a net sink of atmospheric CO_2 with maximum values higher than 50 mmol m^{-2} d^{-1} during the intense summer bloom and with a mean CO_2 sink of 6.9 mmol m^{-2} d^{-1} from late April to September 2012 (at 49.90°N). This extreme CO_2 sink was brief and lasted less than a few days. Only a VOS regularly crossing the WEC would be able to catch the spatial and temporal expansion of this event. At the same time, in the sWEC, surface seawater pCO₂ remained close to, but over, the atmospheric equilibrium and this province acted mainly as a source of CO_2 to the atmosphere with a mean air–sea CO_2 flux value of 0.9 mmol m^{-2} d^{-1} from late April to September (at 48.90°N). By removing the thermal effect on pCO₂ (pCO₂@Tmean, Fig. 5c), we observed that biological processes mainly controlled pCO₂ variability from April to September 2012 in the nWEC. In the sWEC the control of biological processes was less clear and during summer thermodynamic processes mostly controlled pCO₂ variability. These results were in agreement with the observations made in Section 3.3, which indicated that in spring–summer 2012 intense and successive phytoplankton blooms were recorded in the nWEC, whereas biological activity was weak in the sWEC. Remineralization processes started earlier in the sWEC (Fig. 4d) than in the nWEC resulting in increasing surface water pCO₂ (Fig. 5b) and decreasing DO% below 100% (Fig. 3e). In October and November 2012 when organic matter remineralization was at its highest level, pCO₂ and air–sea CO_2 fluxes were homogeneous across the WEC. From the hydrographical properties of the water column (Fig. 5a) it clearly appears that the division of the WEC into two main provinces strongly influenced the spatio-temporal distribution of pCO₂ and air–sea CO_2 fluxes.

To better understand how tidal cycles and phytoplankton blooms impacted air–sea CO_2 fluxes, we extracted high-frequency FerryBox and ancillary data at 48.90°N (well-mixed, sWEC) and at 49.90°N (seasonally stratified, nWEC) from the 3rd of July to the 10th of August (Fig. 6).

At 48.9°N (Fig. 6a), the temperature increased continuously, starting around 14.5 °C and reaching 17 °C in August. During this month DO% remained around 105% and pCO₂ values ranged between 350 µatm and 450 µatm. Chl-a concentration remained low (around 1 µg L^{-1}) except during the two neap tides when we observed values higher than 2 µg L^{-1}. During the neap tides the tidal streams were weaker and thus favoured phytoplankton development in the more stable euphotic zone. At the same time the highest values of DO% (around 115%) and lowest values of pCO₂ (around 350 µatm) were recorded. The difference between the highest pCO₂ values during spring tide and the lowest pCO₂ values during neap tide was approximately 50 µatm. In July, CO_2 emission was therefore generally higher at spring tide with values ranging from 2 to 10 mmol m^{-2} d^{-1} depending on wind speed whereas a drawdown of CO_2 of −5 mmol m^{-2} d^{-1} was observed at neap tide when surface waters were undersaturated in CO_2 compared to the atmosphere. In the sWEC the tidal cycle (neap tide/spring tide) was therefore the main factor controlling phytoplankton abundance, DO% and pCO₂ variability. sWEC waters remained a source of CO_2 to the atmosphere during this period because pCO₂ was mostly driven by higher temperature in summer in the absence of significant biological activity.

At 49.9°N (Fig. 6b), in the seasonally stratified nWEC, the variability of biogeochemical parameters was more contrasted. From the 3rd of July to the 10th of August surface seawater pCO₂ remained under the atmospheric equilibrium and ranged between 350 µtm and 150 µatm with DO% ranging between 105% and 140%. During this month pCO₂ and DO% signals showed opposite dynamics. From early July to mid-July, a first phytoplankton bloom was observed with Chl-a concentration higher than 3 µg L^{-1} and SST around 15.5 °C. During this period DO% increased progressively to reach values of 110% and pCO₂ simultaneously decreased to 300 µatm. At the same time nutrients concentrations were low or totally depleted (Fig. 4) in the nWEC. Salinity decreased in mid-July in the upper nWEC (Figs. 3b and 6b) and might have been linked to nutrient inputs into the system from freshwater discharge. SST then increased abruptly due to intense incident solar radiation and low wind speed, which rapidly warmed the surface layer (Fig. 6b). From Chl-a concentration, no surface phytoplankton bloom was observed during the heating of surface water when photosynthetically active radiation (PAR) values were the highest. However, DO% started to increase significantly during surface water warming, suggesting the biological activity. After this abrupt SST increase, an intense phytoplankton bloom was recorded during 10 days with maximum Chl-a concentrations higher than 8 µg L^{-1}. The lowest pCO₂ and highest DO% values were observed during this bloom in late-July and early-August and the maximum CO_2 sink occurred with values higher than 40 mmol m^{-2} d^{-1}. In the nWEC, tidal cycles did not seem to have any impact on phytoplankton blooms, in contrast to the sWEC. The contrast between nWEC and sWEC air–sea CO_2 fluxes was highly apparent during this month and during the productive period with mean values of −6.9 mmol m^{-2} d^{-1} and 0.9 mmol m^{-2} d^{-1}, respectively. The CO_2 sink recorded from the 27th July to the 7th August had a major impact on the air–sea CO_2 fluxes in the nWEC and accounted for 29% of the CO_2 sink during the productive period (at 49.90°N). Without high-frequency crossing of the VOS, such an event would not have been captured, which would lead to an important underestimation of the CO_2 sink during the productive period in the nWEC.

Fig. 7 shows the variation of mean daily and nightly DO% and pCO₂ over five months at 49.90°N and the difference between daily and nightly air–sea CO_2 flux during this period. We plotted pCO₂ to relate its
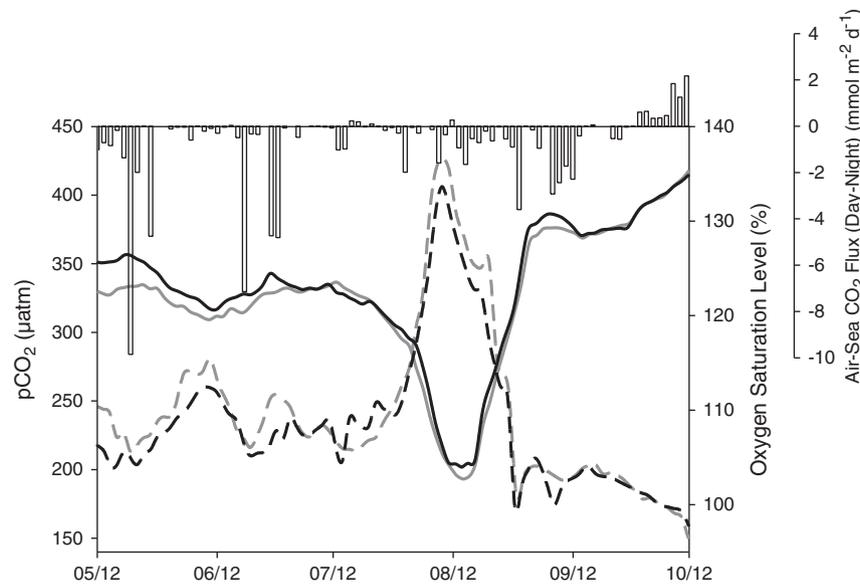
Fig. 5. From the 25th April 2012 to the 1st January 2013, surface distributions of (a) temperature anomaly (°C), (b) pCO₂ (µatm), (c) pCO₂ normalized at the mean temperature of 13 °C (pCO₂@13 °C) from Takahashi et al. (1993) (µatm) and (d) air–sea CO_2 fluxes (mmol m^{-2} d^{-1}) from the algorithm of Nightingale et al. (2000) between Roscoff and Plymouth in the WEC. Negative fluxes indicate a transfer from the atmosphere into the ocean. The black lines represent an estimate of the location of the thermal front; the vertical black lines approximately delimit the period when stratification occurred in the northern WEC.
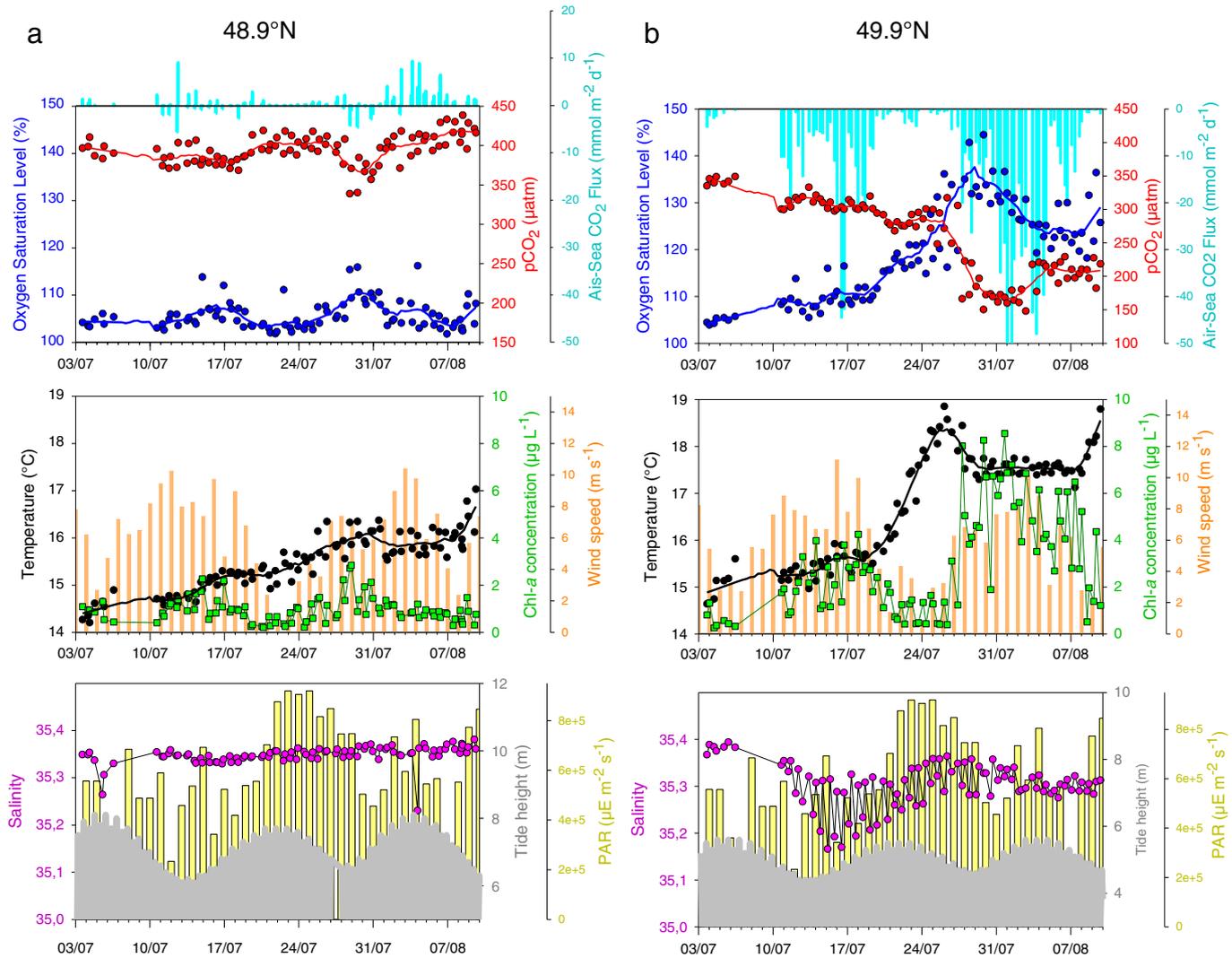
Fig. 6. Extraction of high-frequency FerryBox and ancillary data from the 3rd July to the 10th August at 48.90°N (southern WEC, a) and 49.90°N (northern WEC, b). From the top to the bottom: variations of DO% (blue), pCO₂ (µatm, red) and air–sea CO₂ fluxes (mmol m⁻² d⁻¹, cyan); variations of SST (°C, black), Chl-a concentrations (µg L⁻¹, green) and wind speeds (m s⁻¹, orange); variations of salinity (purple), tide height (m, grey) and daily-integrated photosynthetically active radiation (PAR, µE m⁻² s⁻¹, yellow).

variability directly to diurnal air–sea CO_2 fluxes. It should be noted that pCO_2@Tmean, which is usually plotted versus DO% to evaluate the impact of the diel biological cycle, showed similar variations as pCO_2. Mean DO% during daytime was usually higher than nightly DO% with a maximum difference higher than 6%. An opposite trend was observed for pCO_2 (and pCO_2@Tmean, not shown) with daily values lower than nighttime values with a maximum difference around −30 µatm. Mean DO% and pCO_2 differences between day and night were 2% and −10 µatm from the 25th of April to the 1st of September, respectively. DO% accuracy was 1.2% (at 14 °C and at a salinity of 35.3) considering the 3.3 µmol L⁻¹ standard deviation of the Optode (Section 3.1.), meaning the observed DO% mean difference of 2% was significant. pCO_2 data from the HydroC/CO_2 FT sensor had a standard deviation of 5.2 µatm between discrete and sensor values, therefore the mean day–night difference of −10 µatm was significant. Differences were significant during the productive season (with a range of −1% to 6% for DO% and of −30 to 5 µatm for pCO_2) and allowed us to estimate the impact of the diel biological cycle. During daytime, biological production in surface waters released DO and consumed CO_2, whereas during nighttime respiration was dominant and was responsible for the lower DO% and higher pCO_2 (and pCO_2@Tmean) values recorded. In order to assess the impact of diurnal cycles on air–sea CO_2 exchanges we computed

the difference between daytime and nighttime air–sea CO_2 fluxes. From late April to September the mean day–night air–sea CO_2 flux difference was −0.9 mmol m⁻² d⁻¹ with a minimum value of −10.5 mmol m⁻² d⁻¹. This means that day–night difference accounted for 16% of the mean CO_2 sink during this period and thus was significant for air–sea CO_2 flux computation. These day–night means were calculated from data extracted at 49.90°N and the time of extraction was not always concomitant to the daytime minimum and nighttime maximum pCO_2 values during the diel cycle. These values represent a first estimate of the potential impact of diurnal cycle on air–sea CO_2 fluxes but might be underestimated. Previous studies that specifically investigated the diurnal variability of pCO_2 in a coastal ecosystem based on continuous mooring pCO_2 data reported similar diurnal dynamics. Bozec et al. (2011) reported that monthly air–sea CO_2 flux estimates in the Bay of Brest (France) would be 8 to 36% lower if pCO_2 measurements were made only during the daytime and would be 8 to 37% higher if pCO_2 measurements were made only at nighttime during the productive season. In the nWEC, at Station L4 (50°15.00 N; 4°13.02 W, Fig. 1), Litt et al. (2010) reported pCO_2 variation of 40 µatm between daytime minimum and nighttime maximum over 20 h at a fixed station. Although our high-frequency pCO_2 FerryBox measurements did not cover an entire diel cycle, diurnal biological

Fig. 7. Variations of mean daily (grey) and nightly (black) DO% values (dashed lines) and pCO_2 (μatm) (solid lines) from the 25th April 2012 to the 1st October 2012 at 49.90°N. The bars represent the difference between daily and nightly computed air–sea CO_2 fluxes (mmol m^{-2} d^{-1}) averaged every 3 days.

cycles were observed and our results confirm the necessity to take into account this variability for air–sea CO_2 flux estimates. The high frequency of crossing between Roscoff and Plymouth was an important advantage of this VOS line and allowed us to estimate the potential impact of the biological diel cycle on the air–sea CO_2 fluxes in the WEC.

4. Concluding remarks and perspectives

During the two years of deployment of our FerryBox, we obtained high-frequency data with sufficient precision to investigate the dynamics of biogeochemical processes related to air–sea CO_2 fluxes in the WEC. The SST anomaly was a suitable proxy for precise location of the position of the thermal front, which divided the WEC into two contrasted hydrographical provinces: the seasonally stratified northern WEC and the all-year well-mixed southern WEC. Based on a high-frequency dataset we assessed for the first time the dynamics of phytoplankton blooms and associated biogeochemical processes, which allowed us to develop a better understanding of the spatial and the temporal variability of these events in two contrasted provinces and over two contrasted years. In the sWEC, light availability seemed to be the main factor controlling phytoplankton blooms before total nutrient depletion, whereas tidal cycles (neap/spring tides) appeared to have an influence on phytoplankton abundance. In the nWEC, nutrients (mainly NO_3^-) were totally depleted in both years and were the main limiting factor for phytoplankton blooms. Air–sea CO_2 fluxes were also highly related to the hydrographical properties of the WEC between late April and early September 2012: the sWEC was a weak source of CO_2 to the atmosphere of 0.9 mmol m^{-2} d^{-1}, whereas the seasonally stratified nWEC acted as a sink for atmospheric CO_2 of 6.9 mmol m^{-2} d^{-1}. The necessity to obtain high-frequency observations in coastal ecosystems (as recommended by Borges et al. (2010)) was highlighted in our study by the intense and short (less than 10 days) summer bloom in the nWEC, which contributed to 29% of the CO_2 sink during the productive period. Furthermore, an extraction of day/night data at 49.90°N showed that the mean day/night pCO_2 difference, linked to the diel biological cycle, accounted for 16% of the mean CO_2 sink during the 5 month study period.

Petersen et al. (2011) showed that since FerryBoxes only provide sea surface measurements, a coupling with fixed station profiles can add a new dimension to the VOS routes. Many coastal fixed stations are operated by research institutes to measure common biogeochemical parameters, which could be coupled with FerryBox data to further investigate the pCO_2 dynamics in coastal ecosystems. The two years of deployment of our FerryBox showed that these new instruments are essential tools for future studies of the variability of biogeochemical parameters from diurnal to inter-annual time-scales in dynamic coastal ecosystems such as the WEC. Long-term deployments of FerryBoxes are challenging in terms of maintenance and long term funding, but critical to assess anthropogenic forcings (e.g. ocean acidification, eutrophication) on coastal ecosystems in the context of climate change.

References

Aminot, A., Kérouel, R., 2007. Dosage automatique des nutriments dans les eaux marines. Ed. Quae, 189 p.

Boalch, G.T., Harbour, D.S., Butler, E.I., 1978. Seasonal phytoplankton production in the Western English Channel 1964–1974. J. Mar. Biol. Assoc. UK 58, 943–953.

Borges, A.V., Frankignoulle, M., 2003. Distribution of surface carbon dioxide and air–sea exchange in the English Channel and adjacent areas. J. Geophys. Res. 108.

Borges, A.V., Alin, S.R., Chavez, F.P., Vlahos, P., Johnson, K.S., Holt, J.T., Balch, W.M., Bates, N., Brainard, R., Cai, W.J., 2010. A global sea surface carbon observing system: inorganic and organic carbon dynamics in coastal oceans. In: Hall, J., Harrison, D.E., Stammer, D. (Eds.), Proceedings of OceanObs'09: Sustained Ocean Observations and Information for Society (Vol. 2), Venice, Italy, 21–25 September 2009. ESA Publication WPP-306., Vol. 2.

Bozec, Y., Merlivat, L., Baudoux, A.-C., Beaumont, L., Blain, S., Bucciarelli, E., Danguy, T., Grossteffan, E., Guillot, A., Guillou, J., 2011. Diurnal to inter-annual dynamics of pCO₂ recorded by a CARIOCA sensor in a temperate coastal ecosystem (2003–2009). Mar. Chem. 126, 13–26.

Bozec, Y., Cariou, T., Macé, E., Morin, P., Thuillier, D., Vernet, M., 2012. Seasonal dynamics of air–sea CO₂ fluxes in the inner and outer Loire estuary (NW Europe). Estuar. Coast. Shelf Sci. 100, 58–71.

Dickson, A.G., Millero, F.J., 1987. A comparison of the equilibrium constants for the dissociation of carbonic acid in seawater media. Deep Sea Res. A Oceanogr. Res. Pap. 34, 1733–1743.

Dickson, A.G., Sabine, C.L., Christian, J.R. (Eds.), 2007. Guide to best practices for ocean CO₂ measurements. PICES Special Publication, 3 (191 pp.).

DOE, 1994. Handbook of Methods for the Analysis of the Various Parameters of the Carbon Dioxide System in Sea Water, Version 2.

Dumousseaud, C., Achterberg, E.P., Tyrrell, T., Charalampopoulou, A., Schuster, U., Hartman, M., Hydes, D.J., 2010. Contrasting effects of temperature and winter mixing on the seasonal and inter-annual variability of the carbonate system in the Northeast Atlantic Ocean. Biogeosciences 7, 1481–1492.

Edmond, J., 1970. High precision determination of titration alkalinity and total carbon dioxide content of sea water by potentiometric titration. Deep Sea Res. Oceanogr. Abstr. 17, 737–750.

EPA, 1997. In vitro determination of chlorophyll a and pheophytin a in marine and freshwater algae by fluorescence. In: Arar, E.J., Collins, G.B. (Eds.), Method 445.0, Revision 1.2. US-Environmental Protection Agency, Cincinnati (26 pp.).

Fiedler, B., Fietzek, P., Vieira, N., Silva, P., Bittig, H.C., Körtzinger, A., 2013. In situ CO₂ and O₂ measurements on a profiling float. J. Atmos. Ocean. Technol. 30, 112–126.

Fietzek, P., Körtzinger, A., 2010. Optimization of a membrane-based NDIR sensor for dissolved carbon dioxide. In: Hall, J., Harrison, D.E., Stammer, D. (Eds.), Proceedings of OceanObs'09: Sustained Ocean Observations and Information for Society, Venice, Italy, 21–25 September 2009. ESA Publication WPP-306, vol. 2.

Goberville, E., Beaugrand, G., Sautour, B., Tréguer, P., Team, S., 2010. Climate-driven changes in coastal marine systems of western Europe. Mar. Ecol. Prog. Ser. 408, 129–148.

Guilloux, L., Rigault-Jalabert, F., Jouenne, F., Ristori, S., Viprey, M., Not, F., Vaulot, D., Simon, N., 2013. An annotated checklist of marine phytoplankton taxa at the SOMLIT-Astan time series off Roscoff (western Channel, France): data collected from 2000 to 2010. Cah. Biol. Mar. 54, 247–256.

Hill, A.E., Brown, J., Fernand, L., Holt, J., Horsburgh, K.J., Proctor, R., Raine, R., Turrell, W.R., 2008. Thermohaline circulation of shallow tidal seas. Geophys. Res. Lett. 35.

Hoppe, C.M.J., Langer, G., Rokitta, S.D., Wolf-Gladrow, D.A., Rost, B., 2012. Implications of observed inconsistencies in carbonate chemistry measurements for ocean acidification studies. Biogeosciences 9, 2401–2405.

Hydes, D.J., Hartman, M.C., Kaiser, J., Campbell, J.M., 2009. Measurement of dissolved oxygen using optodes in a FerryBox system. Estuar. Coast. Shelf Sci. 83, 485–490.

Hydes, D.J., Colijn, F., Petersen, W., Mills, F.S.D., Durand, D., NIVA, B.N., 2010. The way forward in developing and integrating FerryBox technologies. Proceedings of OceanObs. 9.

IPCC, Climate Change, 2007. The Physical Science Basis. Contribution of Working Group I to the Fourth Assessment. In: Arar, E.J., Collins, G.B. (Eds.), Report of the Intergovernmental Panel on Climate Change. Edited by: S. Solomon, D. Quin, M. Manning, Z. Chen, M. Marquis.

Kalnay, E., Kanamitsu, M., Kistler, R., Collins, W., Deaven, D., Gandin, L., Iredell, M., Saha, S., White, G., Woollen, J., Zhu, Y., Chelliah, M., Ebisuzaki, W., Higgins, W., Janowlak, J., Mo, K.C., Ropelewski, C., Wang, J., Leetmaa, A., Reynolds, R., Jenne, R., Joseph, D., 1996. The NCEP/NCAR reanalysis project. Bull. Am. Meteorol. Soc. 77, 437–471.

Kelly-Gerreyn, B.A., Hydes, D.J., Jégou, A.M., Lazure, P., Fernand, L.J., Puillat, I., Garcia-Soto, C., 2006. Low salinity intrusions in the western English Channel. Cont. Shelf Res. 26, 1241–1257.

Kitidis, V., Hardman-Mountford, N.J., Litt, E., Brown, I., Cummings, D., Hartman, S., Hydes, D., Fishwick, J.R., Harris, C., Martinez-Vicente, V., Woodward, E.M.S., Smyth, T.J., 2012. Seasonal dynamics of the carbonate system in the Western English Channel. Cont. Shelf Res. 42, 30–40.

Koeve, W., Oschlies, A., 2012. Potential impact of DOM accumulation on fCO2 and carbonate ion computations in ocean acidification experiments. Biogeosciences 9, 3787–3798.

L'Helguen, S., Madec, C., LeCorre, P., 1996. Nitrogen in permanently well-mixed temperate coastal waters. Estuar. Coast. Shelf Sci. 42, 803–818.

Litt, E.J., Hardman-Mountford, N.J., Blackford, J.C., Mitchelson-Jacob, G., Goodman, A., Moore, G.F., Cummings, D.G., Butenschon, M., 2010. Biological control of pCO₂ at station L4 in the Western English Channel over 3 years. J. Plankton Res. 32, 621–629.

Mehrbach, C., Culberso, Ch., Hawley, J.E., Pytkowic, R.M., 1973. Measurement of apparent dissociation constants of carbonic acid in seawater at atmospheric pressure. Limnol. Oceanogr. 18, 897–907.

Nightingale, P.D., Malin, G., Law, C.S., Watson, A.J., Liss, P.S., Liddicoat, M.I., Boutin, J., Upstill-Goddard, R.C., 2000. In situ evaluation of air–sea gas exchange parameterizations using novel conservative and volatile tracers. Glob. Biogeochem. Cycles 14, 373–387.

Omar, A.M., Olsen, A., Johannessen, T., Hoppema, M., Thomas, H., Borges, A.V., 2010. Spatiotemporal variations of fCO₂ in the North Sea. Ocean Sci. 6, 77–89.

Padin, X.A., Vázquez-Rodríguez, M., Ríos, A.F., Pérez, F.F., 2007. Surface CO₂ measurements in the English Channel and Southern Bight of North Sea using voluntary observing ships. J. Mar. Syst. 66, 297–308.

Petersen, W., Schroeder, F., Bockelmann, F.-D., 2011. FerryBox — application of continuous water quality observations along transects in the North Sea. Ocean Dyn. 61, 1541–1554.

Pierrot, D., Lewis, E., Wallace, D.W.R., 2006. MS Excel Program Developed for CO₂ System Calculations. ORNL/CDIAC-105. Carbon Dioxide Information Analysis Center, Oak Ridge National Laboratory, U.S. Department of Energy, Oak Ridge, Tennessee.

Pingree, R., Griffiths, D., 1978. Tidal fronts on shelf seas around British-isles. J. Geophys. Res. C Oceans Atmos. 83, 4615–4622.

Reid, P.C., Auger, C., Chaussepied, M., Burn, M. (Eds.), 1993. The Channel, Report on Sub-region 9, Quality Status Report of the North Sea 1993. UK Dep. of the Environ., Républ. Fr. Minist. de l'Environ., Inst. Fr. de Rech. Pour l'Exploit. de la Mer, Brest (153 pp.).

Saderne, V., Fietzek, P., Herman, P.M.J., 2013. Extreme variations of pCO₂ and pH in a macrophyte meadow of the Baltic Sea in summer: evidence of the effect of photosynthesis and local upwelling. PLoS One 8, e62689.

Schneider, B., Kaitala, S., Maunula, P., 2006. Identification and quantification of plankton bloom events in the Baltic Sea by continuous pCO₂ and chlorophyll a measurements on a cargo ship. J. Mar. Syst. 59, 238–248.

Smyth, T.J., Fishwick, J.R., AL-Moosawi, L., Cummings, D.G., Harris, C., Kitidis, V., Rees, A., Martinez-Vicente, V., Woodward, E.M.S., 2010. A broad spatio-temporal view of the Western English Channel observatory. J. Plankton Res. 32, 585–601.

Southward, A.J., Langmead, O., Hardman-Mountford, N.J., Aiken, J., Boalch, G.T., Dando, P.R., Genner, M.J., Joint, I., Kendall, M.A., Halliday, N.C., Harris, R.P., Leaper, R., Mieszkowska, N., Pingree, R.D., Richardson, A.J., Sims, D.W., Smith, T., Walne, A.W., Hawkins, S.J., 2005. Long-term oceanographic and ecological research in the western English Channel. In: Southward, A.J., Tyler, P.A., Young, C.M., Fuiman, L.A. (Eds.), Adv. Mar. Biol., 47, pp. 1–105.

Takahashi, T., Olafsson, J., Goddard, J.G., Chipman, D.W., Sutherland, S.C., 1993. Seasonal variation of CO2 and nutrients in the high-latitude surface ocean — a comparative study. Glob. Biogeochem. Cycles 7, 843–878.

Wafar, M.V.M., Le Corre, P., Birrien, J.L., 1983. Nutrients and primary production in permanently well-mixed temperate coastal waters. Estuar. Coast. Shelf Sci. 17, 431–446.

Walsh, J.J., 1991. Importance of continental margins in the marine biogeochemical cycling of carbon and nitrogen. Nature 350, 53–55.

Weiss, R.F., 1970. Solubility of nitrogen, oxygen and argon in water and seawater. Deep Sea Res. 17, 721–735.

Weiss, R.F., Price, B.A., 1980. Nitrous oxide solubility in water and seawater. Mar. Chem. 8, 347–359.

Xing, X., Claustre, H., Blain, S., D'Ortenzio, F., Antoine, D., Ras, J., Guinet, C., 2012. Quenching correction for in vivo chlorophyll fluorescence acquired by autonomous platforms: a case study with instrumented elephant seals in the Kerguelen region (Southern Ocean). Limnol. Oceanogr. Methods 10, 483–495.

Zeebe, R.E., Wolf-Gladrow, D.A., 2001. CO₂ in Seawater: Equilibrium, Kinetics, Isotopes. 65. Elsevier Oceanography Series, Amsterdam, (346 pp.).